Geochemistry, Geophysics, Geosystems

RESEARCH ARTICLE
10.1029/2020GC009379

Key Points:

- Brushing and bleach treatments fail to completely remove external contaminants from valve edges and might compromise E/Ca measurements
- Incomplete or juvenile *Krithe* samples often yield less reproducible E/Ca measurements
- *Polycope* ostracodes show promise for Arctic paleotemperature reconstructions

Supporting Information:

- Supporting Information S1

Correspondence to:
C. Not,
cnot@hku.hk

Citation:
Rodriguez, M., Doherty, J. M., Man, H. L. H., Wang, R., Xiao, W., Zhou, B., et al. (2021). Intra-valve elemental distributions in Arctic marine ostracodes: Implications for Mg/Ca and Sr/Ca paleothermometry. *Geochemistry, Geophysics, Geosystems*, *22*, e2020GC009379. https://doi.org/10.1029/2020GC009379

Received 17 AUG 2020
Accepted 26 NOV 2020

Intra-Valve Elemental Distributions in Arctic Marine Ostracodes: Implications for Mg/Ca and Sr/Ca Paleothermometry

Maximiliano Rodriguez[1], John M. Doherty[1], Ho Lai Hilary Man[1], Rujian Wang[2], Wenshen Xiao[2], Baochun Zhou[3], Benoit Thibodeau[1], and Christelle Not[1]

[1]Department of Earth Sciences and Swire Institute of Marine Science, The University of Hong Kong, Hong Kong SAR, Hong Kong, [2]State Key Laboratory of Marine Geology, Tongji University, Shanghai, China, [3]Shanghai Natural History Museum, Branch of Shanghai Science and Technology Museum, Shanghai, China

Abstract Reconstructing intermediate and bottom-water temperature in the Arctic Ocean is key for understanding paleoclimatic phenomena, such as the region's interactions with warm Atlantic waters, stratification, and sea-ice dynamics. However, benthic proxy archives are sparse throughout the Arctic circle compared to lower latitudes. Trace-element ratios (E/Ca) derived from ostracodes, a group of bivalved microscopic crustaceans, have shown promise in this regard. Samples for E/Ca measurements typically require rigorous cleaning prior to analysis, and signs of contamination are routinely monitored through the presence of other trace elements such as Al, Fe, and Mn, which are associated with suspected sources of overprinting. However, there has not yet been an intra-valve investigation of all of these trace elements, which may hinder our ability to effectively identify geochemical overprinting. Here, we present several elemental concentration and E/Ca ratio measurements in two ostracode genera, *Krithe* and *Polycope*, extracted from Chukchi Sea sediment samples. We further investigate the intra-valve distribution of elements within single shells of adult and juvenile specimens using electron probe microanalysis (EPMA). Our findings suggest that brushing and bleach treatments may not be effective for completely eliminating clays from the edges of valves, which can bias paleoclimatologically relevant trace-element proxies such as Mg/Ca ratios, particularly in the case of incomplete or small samples with low amounts of calcite material. In addition, we report the first trace-element data from the genus *Polycope*, which shows potential as a new Arctic paleotemperature archive.

1. Introduction

Characterizing past changes in the Arctic region is critical for understanding geological climate perturbations. Reconstructing intermediate- and bottom-water temperature dynamics are of particular paleoclimatological interest due their relationship to water-mass stratification and consequent impacts on sea-ice variability under past climatic conditions (Cronin et al., 2012). Proxies based on trace-element and isotopic properties of calcium carbonate ($CaCO_3$) biominerals preserved in the geological record have a long and rich history in paleoceanographic research (e.g., Lea, 2013). However, in the Arctic region, geologically relevant marine organisms are scarce and thus microfossil archives are limited to select species of foraminifera (Barrientos et al., 2018; Skirbekk et al., 2016) and ostracodes (Cronin et al., 2017, 2012; Farmer et al., 2012).

Ostracodes, benthic crustaceans whose $CaCO_3$ valves are readily available within Arctic sediment cores, have been previously identified as promising archives for high-latitude bottom-water temperature reconstructions (Cronin et al., 1996; Farmer et al., 2012). For example, Mg/Ca paleothermometry in the genus *Krithe* has been used to infer deep water-mass dynamics in the Arctic region over the last glacial cycle, providing evidence for a deepening of the Atlantic layer (Cronin et al., 2012). Interestingly, this study also highlighted the potential use of strontium (Sr) contained in *Krithe* valves for paleotemperature reconstructions due to a presumed thermodynamically driven incorporation mechanism opposite in sign to that of Mg. More recently, Cronin et al. (2017) applied the ostracode Mg/Ca paleothermometer to characterize changes in the intensification of Arctic amplification since the Mid-Brunhes Event about 400 kyr ago. From a geochemical perspective, marine ostracodes offer two potentially advantageous characteristics over foraminifera. First,

ostracodes tend to incorporate a higher degree of Mg into their valves compared to foraminifera and thus may reasonably be less sensitive to minor diagenetic overprinting (Cronin et al., 1996). Second, the degree of carbonate unsaturation in deep waters imparts an effect on Mg partitioning in benthic foraminifera (Elderfield et al., 2006; Rosenthal et al., 2006), which in some cases operates as the major driver of foraminifer Mg/Ca rather than temperature (Yu & Elderfield, 2008). Such an effect was either not found or found to be of secondary importance in *Krithe* valvesin previous studies (Elmore et al., 2012; Farmer et al., 2012), which suggests that the Mg/Ca ratio of this genus may more faithfully track bottom-water temperature conditions rather than deep-water carbonate chemistry.

However, there are a variety of processes unrelated to the biogenic mineral by which Mg may be introduced to an ostracode valve and thus compromise the paleoceanographic interpretation derived from such a proxy. Specifically, undesired Mg addition may be associated with three dominant sources: 1) organic matter content, derived from both external contaminants and/or from the organism itself, 2) clay contamination, and 3) diagenesis. Detailed analysis of the coordination chemistry within one *Krithe* valve suggests that most of its Mg content is indeed associated with its organic framework (Branson et al., 2018). However, because the organic source is not subject to the same thermodynamic relationship thought to govern Mg incorporation into the carbonate mineral, a failure to remove such a source may add biases to paleotemperature reconstructions. Similarly, clay sourced from the ostracode's original depositional environment may introduce additional Mg-rich particulates into the valve unrelated to temperature conditions, which require sufficient elimination prior to geochemical measurements (e.g., Gray et al., 2014; Jin et al., 2006; Kondo et al., 2005). Finally, several diagenetic processes outlined by Bennett et al. (2011) are associated with both morphological and geochemical alterations of ostracode valves, and must therefore be taken into consideration when applying such proxies to deep-time paleoenvironmental studies.

While most cleaning protocols recommend specific treatments designed to target these presumed sources of undesired Mg (e.g., Gray et al., 2014; Jin et al., 2006; Kondo et al., 2005), there have not yet been any intra-valve studies of key elements commonly used to identify contamination (i.e., Fe, Al, and Mn). Therefore, the extent to which such treatments effectively remove contamination still remains unresolved. Here, we investigated the intra-valve profiles and concentrations of elements in single shells of the two most common ostracode genera in the central Arctic Ocean, *Krithe* and *Polycope* (Gemery et al., 2017), to better assess the efficacy of sample cleaning. In doing so, we identified scenarios under which ostracode Mg/Ca ratios may and may not be reliable for paleotemperature reconstructions. Finally, we present the first trace-element measurements of *Polycope* valves, which show potential promise as future Arctic paleo-archives.

2. Materials and Methods

2.1. Sample Collection

Specimens from two genera of benthic ostracodes, *Krithe* and *Polycope*, were collected from sediment core ARC3-P31 retrieved in 2008 from the Chukchi Plateau (78.012°N–168.016°E) during the CHINARE III expedition (Figure S1; Z. Zhang, 2004). Core ARC3-P31 was collected within the Atlantic layer at a water depth of 434 m. The core is 59 cm in length and consists of two brown units (0–13 cm and 28–59 cm) with a yellowish layer in between (13 and 28 cm). The brown units are enriched in Mn, characteristic of interglacial/interstadial intervals in central Arctic Ocean sediments (e.g. Polyak et al., 2004; Stein et al., 2009; Xiao et al., 2020). A distinct whitish layer occurs at 20 cm core depth, corresponding to a major detrital carbonate discharge event from the Laurentide Ice Sheet (Figure S2; T. Zhang et al., 2019). The core stratigraphy was constrained by 5 AMS ^{14}C dates, showing Holocene and MIS three sedimentation for the two brown units (Figure S2; T. Zhang et al., 2019). In this core, biogenic carbonates are mostly present in interglacial/interstadial sediments, as observed in other cores from the Canada Basin (e.g., Cronin et al., 2014; Marzen et al., 2016; Not & Hillaire-Marcel, 2010). We selected ostracode valves from several different sediment layers where they were most abundant so as to allow for appropriate comparisons between concentration measurements and intra-valve geochemical profiles. These layers were: 6–7 cm, 10–11 cm, 13–14 cm, 21–22 cm, 29–30 cm and 49–50 cm. The quality of our data is discussed in terms of the average standard deviation calculated from all layers, as raw E/Ca ratios may be impacted by different chemical and/or thermal water-mass properties characteristic of different time periods.

2.2. Determination of Elemental Concentrations via ICP-MS

Trace elements were analyzed in individual shells using an Agilent 7900 ICP-MS in the School of Biological Sciences at the University of Hong Kong. *Krithe* and *Polycope* ostracodes were brush-picked from the >150 μm dry fraction under a stereomicroscope. *Krithe* juveniles were identified by their lack of a developed marginal infold. As there are no distinct morphological features between *Polycope* adults and juveniles, it is difficult to assess the molt stage, and so no distinction between adults and juveniles is made here. Valves were carefully examined to avoid carapaces with traces of dissolution. Ostracode specimens were then bleached for >12 h in 5% sodium hypochlorite in order to remove organic matter. Following this, ostracodes were rinsed with milli-Q water three times and then soaked in methanol, rinsed with milli-Q and brushed for 3–5 min to remove clays stuck to the surface. Then, ostracodes were rinsed three times again with milli-Q water. Valves were not sonicated in order to preserve the structural integrity of the specimens. After cleaning, each shell was dissolved with 3–8 mL of 2% nitric acid in a separate tube and analyzed by ICP-MS.

Blanks were measured every three samples to correct for any memory effects during ICP-MS runs. Two multi-element standards prepared from pure solutions and one coral carbonate standard (JCp-1) were analyzed during every run (Inoue et al., 2004; Okai et al., 2002). One multi-element standard was used to correct any biases produced by changes in the calibration curve during the run, while the other two standards were used to test for accuracy and precision. We recorded concentrations of Ca, Mg, Sr, Al, Mn, and Fe. The precision (relative standard deviation; "RSD") and accuracy (difference from the certified value; "Diff") in our measurements for both standards are reported in Table 1. The precision of Mg/Ca and Sr/Ca in JCp-1 was calculated to be 5.1% and 2.3% respectively, while the accuracy was −1.0% and −0.5%, respectively ($n = 104$). The precision of Mg/Ca, Sr/Ca, Fe/Ca, Al/Ca, and Mn/Ca in the multi-element standard was 3.1%, 2.2%, 6.8%, 8.2%, and 2.5% respectively, while the accuracy was −6.2%, −3.4%, −9.3%, −4.1%, and −4.7%, respectively ($n = 106$). The limit of quantification (LoQ) was calculated by Equation 1 (e.g., Keith et al., 1983; Thomsen et al., 2003):

$$\mathrm{LoQ} = \mu + 10\sigma. \tag{1}$$

LoQ for Mg, Sr, Fe, Mn, and Al were 0.30, 0.34, 0.43, 0.28, and 0.34 ug L^{-1}, respectively ($n = 105$).

2.3. SEM Imaging of Ostracode Valves

Valves selected for scanning electron microscope (SEM) imaging were first cleaned following the same protocol as in ICP-MS analysis. The cleaned specimens were attached with double-sided carbon tape to SEM aluminum studs after 1-s immersion in <1% HCl solution following the methodology of De Deckker (2017). Then, valves were coated in a fine gold layer and scanned at 5 kV and 20 kV by a Hitachi S3400 VP SEM. Ultra-high resolution pictures were obtained at 5 kV with a Hitachi S-4800 FEG Scanning Electron Microscope in the Electron Microscope Unit at the University of Hong Kong.

Table 1
Assessment of ICP-MS Precision and Accuracy

	JCp-1 ($n = 104$)			Multi-element standard ($n = 106$)		
Elements	Concentration μg L^{-1}	Precision %	Accuracy %	Concentration, μg L^{-1}	Precision %	Accuracy %
Ca	576.7	2.5	4.0	276.3	2.5	3.6
Mg	1.5	4.9	2.8	5.0	2.9	−2.7
Sr	10.9	1.7	3.4	5.0	1.8	−0.3
Fe	0.04	BLoQ	BLoQ	5.0	7.2	−5.5
Al	0.7	68.9	−37.7	5.0	8.3	−0.6
Mn	0.002	BLoQ	BLoQ	5.0	2.0	−0.9

Note. "BLoQ" indicates scenarios during which the element was below the limit of quantification.

2.4. Determination of Intra-valve Distribution of Elements via EPMA

We produced elemental mappings of 13 ostracode shells, which included cleaned and uncleaned samples of the genera *Krithe* and *Polycope*. Ostracodes for electron proble microanalysis (EPMA) were treated with the same cleaning protocol used for ICP-MS analysis before dissolution. Then, *Krithe* and *Polycope* specimens were placed convex side up or upright perpendicularly on a transparent plate and mounted in epoxy resin, which was polished and carbon-coated in order to remove imperfections and reduce surface brightness. Elemental profiles of ostracodes were mapped using a JEOL JXA-8230 SuperProbe in the Department of Earth Sciences at the University of Hong Kong. We applied a 15-kV accelerating voltage and 20-nA beam current on a 1-μm grid space to measure Mg, Al, Ca, and Fe determined via Kα X-rays in the wavelength-dispersive spectrometry mode. Mg and Al were recorded through a TAP crystal, Ca through a PET crystal and Fe through a LIF crystal using a 100 ms dwell time per pixel. The minimum detection level (MDL) of each element was determined as the smallest peak of the element successfully resolved from the background signal (b), following Equation 2, ensuring the existence of the peak at 99.9% certainty:

$$\mathrm{MDL} = b + 3b^{1/2}. \quad (2)$$

3. Results and Discussion

3.1. Elemental Ratios in *Krithe* Specimens

Mg/Ca and Sr/Ca ratios measured in replicate *Krithe* adults show good intra-layer agreement among each other with the exception of two Mg-enriched outliers from the 6 cm layer (Table 2). Disregarding these anomalous measurements, the average Mg/Ca and Sr/Ca standard deviations (1σ) for adults throughout all sediment layers are 1.1 and 0.2 mmol mol^{-1} respectively, with Mg/Ca ratios ranging from 10.4 to 27.6 mmol mol^{-1} and Sr/Ca ratios ranging from 2.1 to 3.5 mmol mol^{-1}. By comparison, Mg/Ca and Sr/Ca ratios in juvenile specimens of the same genus are considerably more variable, with standard deviations (1σ) across all sediment layers reaching 29.9 and 1.0 mmol mol^{-1} respectively. An exclusion of the anomalously high data from the 21 cm layer changes the standard deviation to 2.3 and 1.1 for Mg/Ca and Sr/Ca, respectively. While limiting measurements to the 10 cm layer enhances juvenile Mg/Ca reproducibility, Mg/Ca and Sr/Ca standard deviations are still ∼2 and 7X larger than adult specimens, respectively. Juvenile Sr/Ca ratios ranged from 0.8 to 3.6 mmol mol^{-1}, with different values compared to Sr/Ca ratios in adults from the same sediment layers, which may indicate the need for different paleotemperature calibrations for different molt stages.

On average, juveniles contained about three times less Ca than adult valves, which may explain their higher E/Ca standard deviations, as low-Ca specimens are more susceptible to E/Ca alterations derived from external sources of trace elements. This could also explain the two adult outliers in the 6 cm layer, as Ca in these specimens contained approximately half of the average adult Ca content. Importantly, this would indicate the need to exercise caution when interpreting trace-metal data in a paleoceanographic framework when using juvenile, incomplete or otherwise low-Ca ostracode shells. Although, because Mg/Ca ratios in adults and juveniles from the 10 cm layer show very similar mean values (11.7 and 12.0 mmol mol^{-1} respectively), juvenile specimens may still be suitable for paleoenvironmental reconstructions if adult specimens are not available, as suggested by Dwyer et al. (2002). However, several replicate valves should be analyzed to ensure that the relatively larger variability is adequately quantified. Moreover, valves from different molt stages should not be mixed as this may lower the reproducibility of paleotemperature reconstructions.

Al/Ca, Fe/Ca, and Mn/Ca are routinely measured to track common sources of contamination in microfossils, and may be sourced from either external particulate such as clay or geochemical alterations of the valve (Barker et al., 2003; Gray et al., 2014). However, in many of our samples these contaminant-associated elements were below the limits of quantification, preventing an accurate calculation of the ratios. As such, the data considered here are derived only from concentrations that were above the limits of quantification, and should therefore be an upper limit of true elemental concentrations and ratios. Al/Ca was considerably lower in adults compared to juveniles (Table 2). By contrast, Fe/Ca was only quantified in two juveniles, which showed high variability. In three out of four adults, Fe/Ca was relatively low, ranging from 0.9 to 1.9 mmol

Table 2
E/Ca Ratios and Elemental Concentrations in Krithe and Polycope ostracodes

Genus	Life stage	MIS	Upper sediment layer (cm)	Mg (ppb)	Mg/Ca (mmol mol^{-1})	Sr (ppb)	Sr/Ca (mmol mol^{-1})	Al (ppb)	Al/Ca (mmol mol^{-1})	Fe (ppb)	Fe/Ca (mmol mol^{-1})	Mn (ppb)	Mn/Ca (mmol mol^{-1})	Ca (ppb)
Krithe	Adult	1	6–7	13.1	11.5	14.1	3.4	1.2	0.9	–	–	BLoQ	BLoQ	1877
				14.1	10.6	16.7	3.5	1.6	1.1	–	–	BLoQ	BLoQ	2,180
				1.0	14.1	0.7	2.5	0.5	6.7	–	BLoQ	BLoQ	BLoQ	109
				60.4	305.9	1.5	2.1	–	–	–	–	–	–	326
				2.6	11.8	2.5	3.1	0.8	3.6	–	–	BLoQ	BLoQ	366
				2.8	11.8	2.5	2.9	1.0	3.5	–	–	BLoQ	BLoQ	394
				58.4	296.5	1.5	2.2	–	–	–	–	–	–	325
				4.2	11.7	4.1	3.2	1.0	2.5	1.8	2.2	BLoQ	BLoQ	590
				4.5	13.2	3.5	2.8	1.0	2.6	14.1	18.3	0.50	0.7	559
			Average	6.0	12.1	6.3	3.1	1.0	3.0	8.0	10.3	0.5	0.7	868
			SD	5.3	1.1	6.3	0.3	0.3	1.9	8.7	11.4	–	–	813
			10–11	4.1	10.6	4.3	3.1	0.7	1.6	0.8	0.9	BLoQ	BLoQ	599
				1.6	11.4	1.6	3.2	0.5	3.5	19.5	61.2	BLoQ	BLoQ	223
				7.6	10.9	8.3	3.3	1.2	1.5	1.6	1.0	BLoQ	BLoQ	1,156
				4.0	14.0	3.0	2.9	1.4	4.2	1.3	1.9	BLoQ	BLoQ	472
			Average	4.3	11.7	4.3	3.1	1.0	2.7	5.8	16.3	–	–	612
			SD	2.5	1.6	2.9	0.2	0.4	1.4	9.1	30.0	–	–	394
		1/2	13–14	4.3	12.1	3.8	3.0	1.0	2.4	–	–	BLoQ	BLoQ	596
				2.7	13.1	2.4	3.3	0.9	3.9	3.8	8.0	BLoQ	BLoQ	335
			Average	3.5	12.6	3.1	3.1	0.9	3.1	3.8	8.0	–	–	465
			SD	1.2	0.7	1.0	0.2	0.1	1.1	–	–	–	–	184
		2	21–22	5.6	27.6	2.0	2.8	1.0	5.0	1.5	3.5	BLoQ	BLoQ	336
		2/3	29–30	2.8	22.1	1.5	3.2	0.8	6.5	BLoQ	BLoQ	BLoQ	BLoQ	212
		3	49–50	4.5	10.4	4.1	2.7	1.8	4.4	1.7	1.9	BLoQ	BLoQ	707
			Average SD (all layers)	***3.0***	***1.1***	***3.4***	***0.2***	***0.3***	***1.5***	***8.9***	***20.7***	**–**	**–**	***464***
	Juvenile	1	10–11	0.6	10.3	0.7	3.6	BLoQ	BLoQ	BLoQ	BLoQ	BLoQ	BLoQ	92
				1.9	13.2	0.8	1.5	0.9	5.9	BLoQ	BLoQ	BLoQ	BLoQ	234
				0.6	9.8	0.5	2.4	BLoQ	BLoQ	BLoQ	BLoQ	BLoQ	BLoQ	92
				0.6	14.7	BLoQ	1.0	0.9	20.6	BLoQ	BLoQ	BLoQ	BLoQ	72
			Average	0.9	12.0	0.7	2.1	0.9	13.3	–	–	–	–	123
			SD	0.6	2.3	0.2	1.1	0.0	10.4	–	–	–	–	75
		2	21–22	25.2	127.4	0.5	0.8	5.3	23.8	8.6	18.9	0.3	0.8	327
				7.6	46.2	1.2	2.0	0.5	2.7	0.9	2.5	BLoQ	BLoQ	273
			Average	16.4	86.8	0.9	1.4	2.9	13.2	4.8	10.7	0.3	0.8	300
			SD	12.4	57.5	0.5	0.9	3.4	14.9	5.5	11.6	–	–	38
			Average SD (all layers)	***6.5***	***29.9***	***0.3***	***1.0***	***1.7***	***12.6***	***5.5***	***11.6***	**–**	**–**	***56***

Table 2
Continued

Genus	Life stage	MIS	Upper sediment layer (cm)	Mg (ppb)	Mg/Ca (mmol mol^{-1})	Sr (ppb)	Sr/Ca (mmol mol^{-1})	Al (ppb)	Al/Ca (mmol mol^{-1})	Fe (ppb)	Fe/Ca (mmol mol^{-1})	Mn (ppb)	Mn/Ca (mmol mol^{-1})	Ca (ppb)
Polycope	N/A	1	6–7	3.5	28.8	2.0	4.6	BLoQ	BLoQ	BLoQ	BLoQ	BLoQ	BLoQ	199
				9.4	30.7	4.7	4.3	BLoQ	BLoQ	BLoQ	BLoQ	BLoQ	BLoQ	506
				8.9	29.6	4.4	4.0	BLoQ	BLoQ	BLoQ	BLoQ	BLoQ	BLoQ	497
			Average	7.3	29.7	3.7	4.3	–	–	–	–	–	–	401
			SD	3.3	0.9	1.5	0.3	–	–	–	–	–	–	175
			10–11	7.9	33.7	3.2	3.8	0.4	1.4	BLoQ	BLoQ	BLoQ	BLoQ	385
				2.1	28.2	0.9	3.2	BLoQ	BLoQ	BLoQ	BLoQ	BLoQ	BLoQ	123
				1.0	27.3	0.5	4.0	BLoQ	BLoQ	BLoQ	BLoQ	BLoQ	BLoQ	58
				2.4	32.2	1.3	4.9	BLoQ	BLoQ	BLoQ	BLoQ	BLoQ	BLoQ	124
			Average	3.3	30.4	1.5	4.0	0.4	1.4	–	–	–	–	172
			SD	3.1	3.1	1.2	0.7	–	–	–	–	–	–	145
		2	21–22	7.0	49.7	1.0	2.0	0.7	4.3	0.6	1.9	BLoQ	BLoQ	232
				11.1	69.4	1.5	2.5	1.4	7.6	1.1	2.9	BLoQ	BLoQ	264
			Average	9.1	59.5	1.2	2.2	1.0	6.0	0.9	2.4	–	–	248
			SD	2.9	14.0	0.3	0.4	0.5	2.4	0.3	0.7	–	–	23
		2/3	29–30	10.6	37.3	3.5	3.4	0.8	2.5	2.1	3.2	BLoQ	BLoQ	466
		3	49–50	1.5	28.4	0.9	4.4	BLoQ	BLoQ	BLoQ	BLoQ	BLoQ	BLoQ	90
				3.6	28.5	1.8	3.9	1.0	7.2	0.8	2.9	BLoQ	BLoQ	209
			Average	2.6	28.4	1.3	4.2	1.0	7.2	0.8	2.9	–	–	149
			SD	1.5	0.1	0.6	0.4	–	–	–	–	–	–	84
			Average SD (all layers)	**2.7**	***4.5***	***0.9***	***0.4***	***0.5***	***2.4***	***0.3***	***0.7***	–	–	***107***

Note that the two low-Ca adult Krithe valves from the 6 cm sediment layer were not included in standard deviation calculations presented on the table.
Note that the juvenile measurements from the 10-11 cm layer were not included in standard deviation calculations presented on the table.
BLoQ, below the limit of quantification; SD, standard deviation.

mol^{-1} with the exception of one anamolously high specimen (61.2 mmol mol^{-1}) in an adult from the 10 cm layer. Interestingly, the large Fe/Ca ratio does not correspond to considerable changes in the specimen's Mg/Ca and Sr/Ca ratios relative to other adults from the same layer (Mg/Ca = 11.4 mmol mol^{-1} in the high-Fe/Ca specimen compared to 10.6, 10.9, and 14.0 mmol mol^{-1} in the others; Sr/Ca = 3.2 mmol mol^{-1} in the high-Fe/Ca specimen compared to 3.1, 3.3, and 2.9 mmol mol^{-1} in the others). This suggests that increased Fe does not always result in E/Ca overprinting. Manganese was below the LoQ in all but one *Krithe* adult and one *Krithe* juvenile and as such is not further discussed.

3.2. Elemental Ratios in *Polycope* Specimens

Compared to *Krithe* adults, *Polycope* specimens generally show higher Mg/Ca ratios (27.3–69.4 mmol mol^{-1}), higher Sr/Ca ratios (2.0–4.9 mmol mol^{-1}), and lower concentrations of Ca (with an average of ~263 ug L^{-1}). These higher Mg/Ca values are similar to those of other ostracode genera from lower latitudes, such as *Loxoconcha* and *Cytheropteron* (Yamada et al., 2014). The average *Polycope* Mg/Ca standard deviation across all sediment layers is 4.5 mmol mol^{-1}, compared to 1.1 mmol mol^{-1} calculated from Mg/Ca ratios in *Krithe* adults (Table 2). However, such a high standard deviation is driven by two shells from the 21 cm layer. By contrast, the average *Polycope* Sr/Ca standard deviation is 0.4 mmol mol^{-1} across all sediment

layers, compared to 0.2 mmol mol^{-1} calculated from Sr/Ca ratios in *Krithe* adults. The relatively higher Mg/Ca standard deviation may caution against applying this conventional paleotemperature proxy to *Polycope* valves. However, the good agreement among intra-layer Mg/Ca (except for the 21 cm layer) and Sr/Ca ratios suggests that *Polycope* Mg/Ca and Sr/Ca ratios may be promising alternative paleotemperature proxies as suggested by Cronin et al. (2012) for *Krithe* ostracodes. Compared to *Krithe* adults and juveniles, *Polycope* valves also generally contain lower Fe/Ca ratios. *Polycope* valves had slightly higher Al/Ca ratios than *Krithe* adults, but lower Al/Ca ratios than *Krithe* juveniles. Given that Al could reflect contamination, these Al/Ca offsets between *Polycope* valves and *Krithe* adults could be due to enhanced particle adherence and/or relatively lower effectiveness in cleaning *Polycope* valves.

3.3. Comparison with Previous Arctic *Krithe* E/Ca Measurements

While there have been several previous Arctic paleoclimate studies based on Mg/Ca ratios in *Krithe* ostracodes (Cronin et al., 1996; Cronin et al., 2012; Farmer et al., 2011), these specimens were picked from cores at different sites, water depths and/or time intervals which could all limit the reliability of any comparison between our data and the previously published data. Moreover, slightly different cleaning (i.e., the use of sonication) and picking (i.e., the possible combination of adult and juvenile specimens) protocols may further complicate such comparisons. However, the mean Mg/Ca value reported from Cronin et al. (2012)'s modern pan-Arctic data compilation agrees well with our results from near-surface adult (6–7 cm; ~7 ka) and juvenile (10–11 cm; ~8–9 ka) specimens (Table 3). In Cronin et al.'s (2012) multi-site study, the variability over the last ~10 ka was generally within 1σ of the mean. Thus, the agreement between our older measurements and those from the pan-Arctic analysis is reasonable, and improves confidence in both analyses despite differences in cleaning procedures. In addition, Farmer et al. (2011) reported lower Mg/Ca values (colder temperature conditions) from a nearby core raised from the shallower polar mixed-layer water depth of 203 m. Because our core was extracted from a water depth corresponding to the relatively warmer Atlantic layer, this offset matches the modern hydrographic temperature profile of the region. While our adult Sr/Ca values also agree with those from the pan-Arctic region, juvenile Sr/Ca ratios on average are 1.1 mmol mol^{-1} lower. This could indicate the need for a juvenile-specific calibration curve, a shortcoming of this potential paleo-temperature proxy and/or its relatively higher susceptibility to contamination. Lower juvenile reproducibility is in line with former cleaning tests, suggesting that sonication was a critical step for removing clay-induced E/Ca overprinting in juvenile *Krithe* (Gray et al., 2014). However, as juvenile specimens were limited from this sediment interval ($n = 4$), we caution against making definitive conclusions based on our observations and encourage future investigations of Sr/Ca ratios in Arctic *Krithe* juveniles.

3.4. Crystallography and Intra-valve Geochemistry

Krithe and *Polycope* specimens selected for SEM imaging show different crystal structures. *Polycopes* are composed of an amorphous crystal matrix (Figure 1), while *Krithe* specimens show better-defined calcite structures. However, the inner sections of *Krithe* valves also appear amorphous, which is typically observed

Table 3
Compilation of Arctic Krithe Mg/Ca and Sr/Ca Ratios From Upper/Surface sediments

Valve type	Region	Depth (m)	Age (ka)	Mg/Ca (mmol mol^{-1})	BWT (°C)	Sr/Ca (mmol mol-1)	Reference
Krithe adults *(n = 7)*	Chukchi Sea	434 (AL)	7	12.1 ± 1.1	0.17	3.1 ± 0.4	This study
Krithe juveniles ($n = 4$)	Chukchi Sea	434 (AL)	8–9	12.0 ± 2.3	0.13	2.1 ± 1.1	This study
Krithe ($n = 12$)	Chukchi Sea	203 (PML)	7–8	7.6 ± 1.1	−1.80	-	Farmer et al. (2011)
Krithe (n = 39)	Pan-Arctic	multiple	Modern	12.7 ± 2.6	0.44	3.1 ± 0.1	Cronin et al. (2012)

Note. Depth acronym "AL" indicates a core extracted from within the Atlantic layer depth whereas "PML" indicates a core extracted from the polar mixed-layer depth. BWT was calculated using mean Mg/Ca values using the Arctic calibration equation given by Farmer et al. (2012).

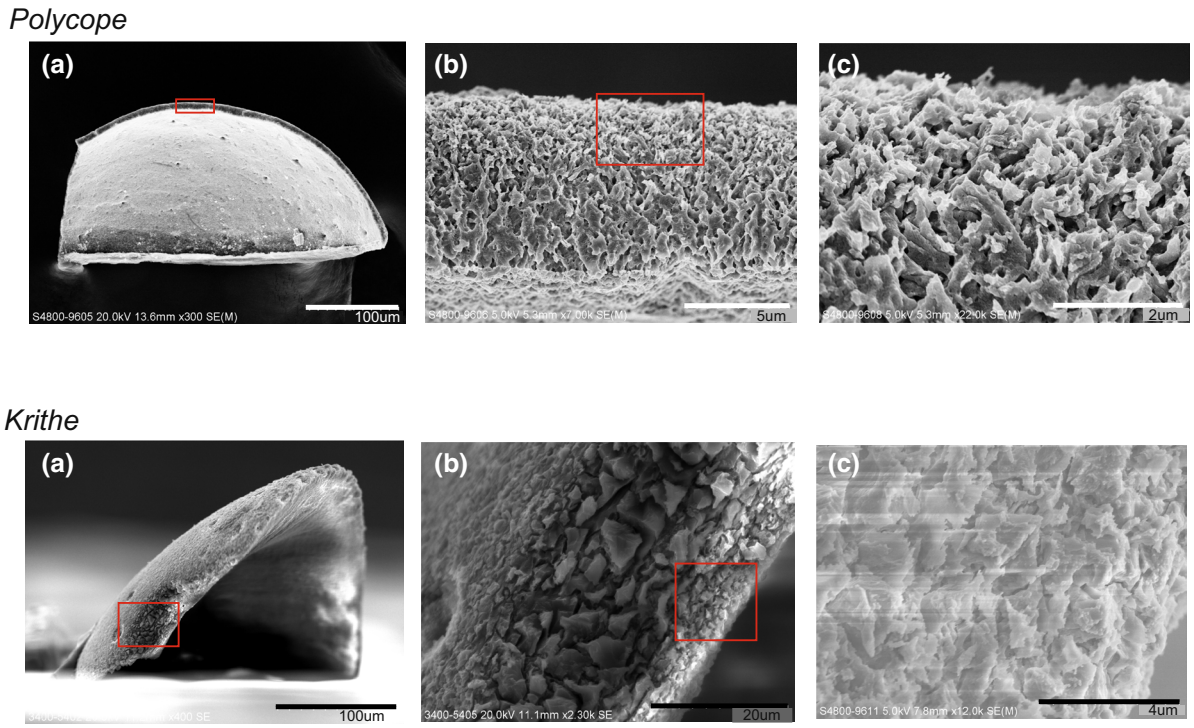

Figure 1. SEM images of *Polycope* (top) and *Krithe* (bottom) shells. (a, b and c) refer to different magnifications of the same shell with the rectangles indicating the area displayed in the next-highest magnification picture. SEM, scanning electron microscope.

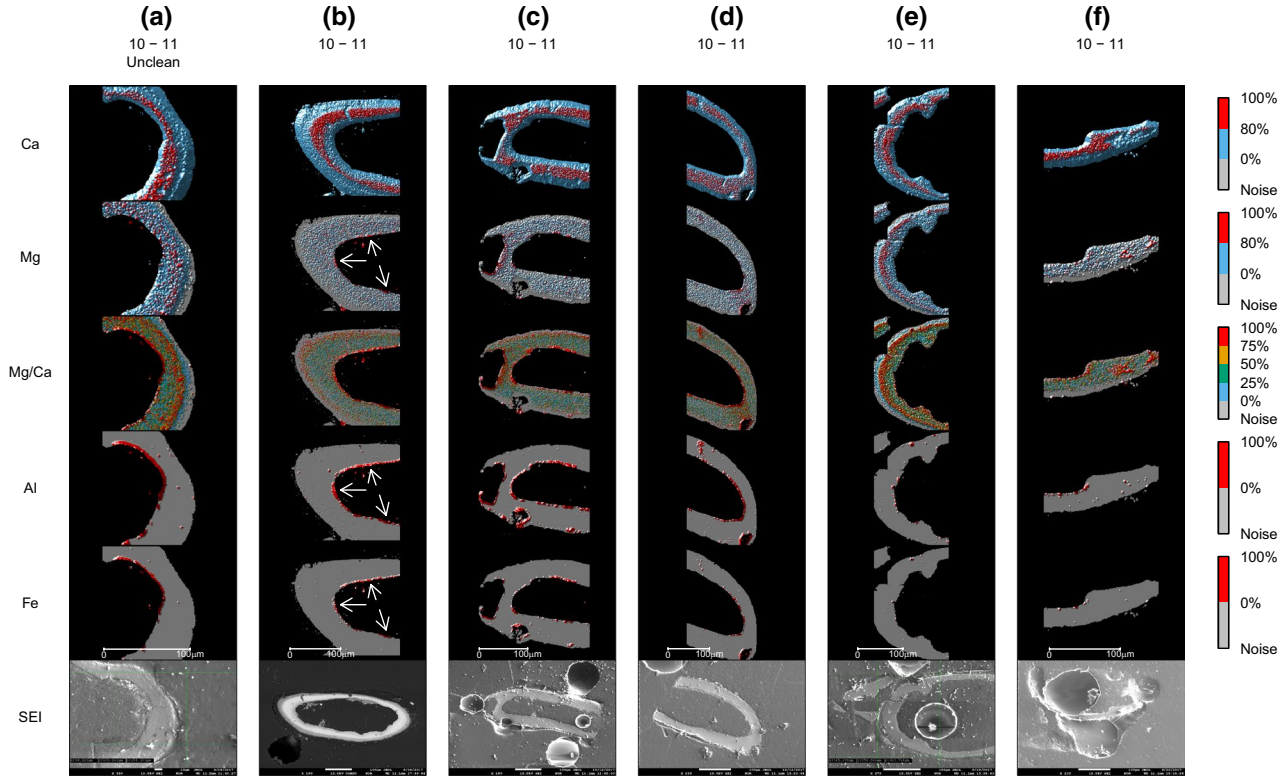

Figure 2. Intra-valve elemental distributions in (a) uncleaned and (b-f) cleaned Krithe adults. Numbers represent the sediment layer and color bars represent the intensity for each element. Elemental units are in percentiles of intensity (see Figure S2 for details regarding the percentile scale). Only the elemental presence is shown for Al and Fe (i.e., 100% of the intensity shown).

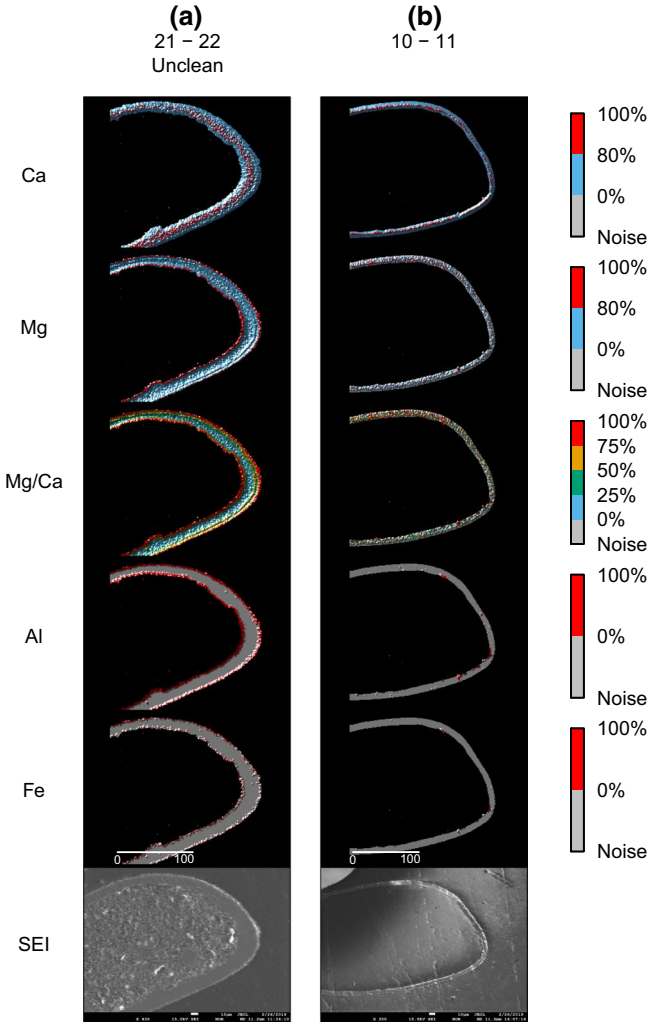

Figure 3. Intra-valve elemental distributions in (a) uncleaned and (b) cleaned Krithe juveniles. The internal intensity in picture (a) was removed to facilitate the visualization of the elemental distribution surrounding valve edges. Elemental units are in percentiles of intensity (see Figure S2 for details regarding the percentile scale). Only the elemental presence is shown for Al and Fe (i.e., 100% of the intensity shown).

during shell calcification after the disintegration of calcium phosphate granules which transform into small granular structures of calcium carbonate (Keyser & Walter, 2004). EPMA images reveal that uncleaned specimens of both genera and molt stages generally contain more areas with Fe and Al compared to cleaned valves, confirming that Fe and Al are effective at tracing contamination (Figures 2–4). Notably, Fe and Al were almost completely eliminated in only one cleaned *Polycope* valve (Figure 4c). Ca concentrations are heterogeneously distributed throughout the valve in cleaned adult and juvenile specimens of *Krithe* (Figures 2 and 3) and *Polycope* (Figure 4), with maximum intensities occurring along a central band in all specimens. Similar Ca distributions were previously observed in *Krithe* valves extracted off northwestern Western Australia (De Deckker, 2017). By contrast, maximum Mg and Mg/Ca intensities are commonly distributed along the edges of cleaned valves in all specimens investigated. The elemental heterogeinity of the shell has been previously suggested as a potential limitation of this proxy (Branson et al., 2018; Morishita et al., 2007). This pattern reveals an additional shortcoming for the use of incomplete ostracode valves in paleoenvironmental research, as the portion of the valve selected for the analysis may not be representative of the full specimen's Mg and/or Ca concentrations and thus bias the Mg/Ca ratio.

Al and Fe are also heterogeneously distributed in *Krithe* and *Polycope* specimens, with highest intensities occurring along the same edge areas that show selective Mg and Mg/Ca enrichment as indicated by the arrows in Figure 2b. Thus, it appears that these elements share a common source. In the central Chukchi Sea, sedimentary Fe content reaches its regional maximum (>10%) due to the presence of Fe-rich pelite muds, which would also presumably contain Al and Mg (Pavlidis et al., 1996). As such, the insufficient removal of these clays from the valve could explain the trace-element profiles of ostracodes from this region. Despite the geochemical agreements between regional clays and anomalous E/Ca content in our samples, diagenesis could have also been important for driving E/Ca variations (Bennett et al., 2011). However, EPMA images suggest that Al and Fe are not housed within the calcite structure of the valve (Figures 2–4), indicating that these elements were likely sourced from post-depositional input rather than geochemical alterations of the shell. Additionally, EPMA images of a cleaned (Figure 2e) and uncleaned (Figure 2a) valve from the same specimen indicate a higher presence of Al and Fe in the latter, which further supports external contamination as a driving mechanism. Moreover, SEM images of *Krithe* ostracodes indicate that cleaned valves are composed of mostly unaltered calcite crystals (Figure 2), and so diagenesis is not a likely explanation for these or other geochemical anomalies. As such, clay contamination is most strongly implicated as the source of elevated Al and Fe, which is also likely responsible for additional Mg content. The additional Mg content associated with external contaminants may be responsible for driving lower Mg/Ca reproducibility in low-Ca ostracodes (Table 2).

4. Conclusions

E/Ca ratios measured from ostracode valves are often used for reconstructing bottom-water ocean temperature. However, the heterogeneous intra-valve distributions of Mg and Ca within ostracodes prevent the effective application of the conventional Mg/Ca proxy to incomplete shell material. In addition, low-Ca *Krithe* specimens are further shown to be occasionally unreliable for Mg/Ca- and, to a lesser degree, Sr/Ca-based paleoenvironmental studies, which is hypothesized to be a result of their very low Ca content and, thus,

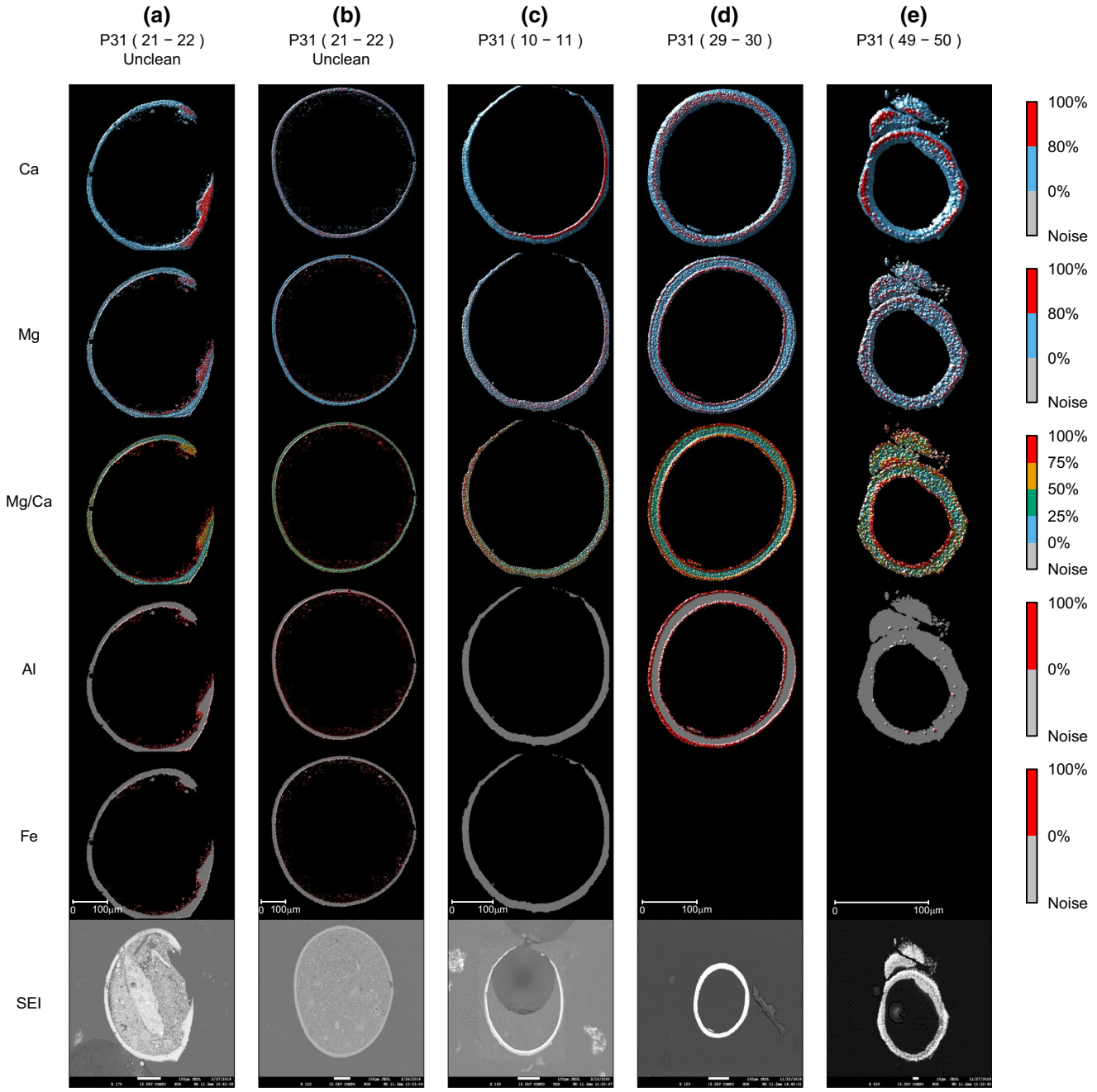

Figure 4. Intra-valve elemental distributions in (a-b) uncleaned and (c-e) cleaned Polycope specimens. The internal intensity in pictures (a) and (b) was removed to facilitate the visualization of the elemental distribution surrounding valve edges. Elemental units are in percentiles of intensity (see Figure S2 for details regarding the percentile scale). Only the elemental presence is shown for Al and Fe (i.e., 100% of the intensity shown).

their high sensitivity to E/Ca overprinting via external contamination. If adult valves are absent, it may be possible to achieve reliable paleoenvironmental estimates from juveniles or other low-Ca valves, but ideally such measurements should be conducted on several replicates to ensure that the relatively higher variability is adequately quantified. Contrastingly, *Polycope* specimens show good reproducibility in E/Ca ratios despite relatively low Ca content, which suggests that this genus may be useful as a new paleotemperature archive in the Arctic region. However, future research is required for the development of a genus-specific calibration curve.

Data Availability Statement

All data are archived and available via the EarthChem Library following link https://doi.org/10.26022/IEDA/111765.

Acknowledgments
This work was supported by the Research Grant Council of Hong Kong under the Early Career Fund (#27302618) and the Seed Funding Program for basic research of the University of Hong Kong (#201611159170) granted to Christelle Not. H. L. H. Man's visit to Tongji University and Shanghai Natural History Museum were funded by the Pilot scheme on International Experiences for research post-graduate students 2016/17 of The University of Hong Kong. Additionally, this work was funded by the Chinese NSF (No. 41776187 and 41030859). The TJ SKLopen fund can be also acknowledged. This work is a contribution to the 3rd Chinese National Arctic Research Expeditions (CHINARE-208) conducted by R/V Xuelong. The authors thank the core repository of the Polar Research Institute of China for providing the sediment samples. Finally, we want to thanks Jesse Farmer and an anymous reviewer for their comments on the ealier version of the manuscript.

References

Barker, S., Greaves, M., & Elderfield, H. (2003). A study of cleaning procedures used for foraminiferal Mg/Ca paleothermometry. *Geochemistry, Geophysics, Geosystems*, *4*(9), 1–20. https://doi.org/10.1029/2003GC000559

Barrientos, N., Lear, C. H., Jakobsson, M., Stranne, C., O'Regan, M., Cronin, T. M., et al. (2018). Arctic Ocean benthic foraminifera Mg/Ca ratios and global Mg/Ca-temperature calibrations: New constraints at low temperatures. *Geochimica et Cosmochimica Acta*, *236*, 240–259. https://doi.org/10.1016/j.gca.2018.02.036

Bennett, C. E., Williams, M., Leng, M. J., Siveter, D. J., Davies, S. J., Sloane, H. J., & Wilkinson, I. P. (2011). Diagenesis of fossil ostracods: Implications for stable isotope based palaeoenvironmental reconstruction. *Palaeogeography, Palaeoclimatology, Palaeoecology*, *305*(1–4), 150–161. https://doi.org/10.1016/j.palaeo.2011.02.028

Branson, O., Redfern, S. A. T., Elmore, A. C., Read, E., Valencia, S., & Elderfield, H. (2018). The distribution and coordination of trace elements in Krithe ostracods and their implications for paleothermometry. *Geochimica et Cosmochimica Acta*, *236*, 230–239. https://doi.org/10.1016/j.gca.2017.12.005

Cronin, T. M., DeNinno, L. H., Polyak, L., Caverly, E. K., Poore, R. Z., Brenner, A., et al. (2014). Quaternary ostracode and foraminiferal biostratigraphy and paleoceanography in the western Arctic Ocean. *Marine Micropaleontology*, *111*, 118–133. https://doi.org/10.1016/j.marmicro.2014.05.001

Cronin, T. M., Dwyer, G. S., Baker, P. A., Rodriguez-Lazaro, J., & Briggs, W. M. (1996). *Deep-sea ostracode shell chemistry (Mg:Ca ratios) and Late Quaternary Arctic Ocean history*. In Geological Society, London: Special Publications. https://doi.org/10.1144/GSL.SP.1996.111.01.08

Cronin, T. M., Dwyer, G. S., Caverly, E. K., Farmer, J., DeNinno, L. H., Rodriguez-Lazaro, J., & Gemery, L. (2017). Enhanced Arctic Amplification Began at the Mid-Brunhes Event ~400,000 years ago. *Scientific Reports*, *7*(1), 1–7. https://doi.org/10.1038/s41598-017-13821-2

Cronin, T. M., Dwyer, G. S., Farmer, J., Bauch, H. A., Spielhagen, R. F., Jakobsson, M., et al. (2012). Deep Arctic Ocean warming during the last glacial cycle. *Nature Geoscience*, *5*(9), 631–634. https://doi.org/10.1038/ngeo1557

De Deckker, P. (2017). Trace elemental distribution in ostracod valves. From solution ICPMS and laser ablation ICPMS to microprobe mapping: A tribute to Rick Forester. *Hydrobiologia*, *786*(1), 23–39. https://doi.org/10.1007/s10750-015-2534-4

Elderfield, H., Yu, J., Anand, P., Kiefer, T., & Nyland, B. (2006). Calibrations for benthic foraminiferal Mg/Ca paleothermometry and the carbonate ion hypothesis. *Earth and Planetary Science Letters*, *250*(3—4), 633–649. https://doi.org/10.1016/j.epsl.2006.07.041

Elmore, A. C., Sosdian, S., Rosenthal, Y., & Wright, J. D. (2012). A global evaluation of temperature and carbonate ion control on Mg/Ca ratios of ostracoda genus Krithe. *Geochemistry Geophysics Geosystems*, *13*(9), 1–20. https://doi.org/10.1029/2012GC004073

Farmer, J. R., Cronin, T. M., De Vernal, A., Dwyer, G. S., Keigwin, L. D., & Thunell, R. C. (2011). Western Arctic Ocean temperature variability during the last 8000 years. *Geophysical Research Letters*, *38*(24), 1–6. https://doi.org/10.1029/2011GL049714

Farmer, J. R., Cronin, T. M., & Dwyer, G. S. (2012). Ostracode Mg/Ca paleothermometry in the North Atlantic and Arctic oceans: Evaluation of a carbonate ion effect. *Paleoceanography*, *27*, 1–14. https://doi.org/10.1029/2012PA002305

Gemery, L., Cronin, T. M., Poirier, R. K., Pearce, C., Barrientos, N., O'Regan, M., et al. (2017). Central Arctic Ocean paleoceanography from ~50 ka to present, on the basis of ostracode faunal assemblages from the SWERUS 2014 expedition. *Climate of the Past*, *13*, 1473–1489. https://doi.org/10.5194/cp-13-1473-2017

Gray, W., Holmes, J., & Shevenell, A. (2014). Evaluation of foraminiferal trace element cleaning protocols on the Mg/Ca of marine ostracod genus Krithe. *Chemical Geology*, *382*, 14–23. https://doi.org/10.1016/j.chemgeo.2014.05.022

Inoue, M., Nohara, M., Okai, T., Suzuki, A., & Kawahata, H. (2004). Concentrations of Trace Elements in Carbonate Reference Materials Coral JCp-1 and Giant Clam JCt-1 by Inductively Coupled Plasma-Mass Spectrometry. *Geostandards and Geoanalytical Research*, *28*(3), 411–416. https://doi.org/10.1111/j.1751-908X.2004.tb00759.x

Jin, Z., Bickle, M., Chapman, H., Yu, J., Greaves, M., Wang, S., & Chen, S. (2006). *An experimental evaluation of cleaning methods for fossil ostracod Mg/Ca and Sr/Ca determination*. Handbook of Environmental Chemistry (Vol. 5). Water Pollution. https://doi.org/10.1007/s10933-006-9007-8

Keith, L. H., Crummett, W., Deegan, J., Libby, R. A., Wentler, G., & Taylor, J. K. (1983). Principles of environmental analysis. *Analytical Chemistry*, *55*(14), 2210–2218. https://doi.org/10.1021/ac00264a003

Keyser, D., & Walter, R. (2004). Calcification in ostracodes. *Revista Espanola de Micropaleontologia*, *36*(1), 1–11.

Kondo, H., Toyofuku, T., & Ikeya, N. (2005). Mg/Ca ratios in the shells of cultured specimens and natural populations of the marine ostracode Xestoleberis hanaii (Crustacea). *Palaeogeography, Palaeoclimatology, Palaeoecology*, *225*, 1–13. https://doi.org/10.1016/j.palaeo.2004.05.026

Lea, D. W. (2013). *Elemental and Isotopic Proxies of Past Ocean Temperatures*. In Treatise on Geochemistry (2nd ed.). Elsevier Science. https://doi.org/10.1016/B978-0-08-095975-7.00614-8

Marzen, R. E., DeNinno, L. H., & Cronin, T. M. (2016). Calcareous microfossil-based orbital cyclostratigraphy in the Arctic Ocean. *Quaternary Science Reviews*, *149*, 109–121. https://doi.org/10.1016/j.quascirev.2016.07.004

Morishita, T., Tsurumi, A., & Kamiya, T. (2007). Magnesium and strontium distributions within valves of a recent marine ostracode, Neonesidea oligodentata: Implications for paleoenvironmental reconstructions. *Geochemistry, Geophysics, Geosystems*, *8*(7), 1–11. https://doi.org/10.1029/2007GC001585

Not, C., & Hillaire-Marcel Claude, C. (2010). Time constraints from 230Th and 231Pa data in late Quaternary, low sedimentation rate sequences from the Arctic Ocean: An example from the northern Mendeleev Ridge. *Quaternary Science Reviews*, *29*, 3665–3675. https://doi.org/10.1016/j.quascirev.2010.06.042

Okai, T., Suzuki, A., Kawahata, H., Terashima, S., & Imai, N. (2002). Preparation of a new Geological Survey of Japan geochemical reference material: Coral JCp-1. *Geostandards newsletter*, *26*(1), 95–99. https://doi.org/10.1111/j.1751-908X.2002.tb00627.x

Pavlidis, Y. A., Ogorodnikov, V. I., Shelekhova, E. S., & Washner, M. (1996). Lithology and geochemistry of modern sediments of the Chukchi Sea. In *Surface-sediment composition and sedimentary processes in the central Arctic Ocean and along the Eurasian continental margin* (pp. 119–125). Berichte zur Polarforschung (Reports on Polar Research).

Polyak, L., Curry, W. B., Darby, D. A., Bischof, J., & Cronin, T. M. (2004). Contrasting glacial/interglacial regimes in the western Arctic Ocean as exemplified by a sedimentary record from the Mendeleev Ridge. *Palaeogeography, Palaeoclimatology, Palaeoecology*. https://doi.org/10.1016/S0031-0182(03)00661-8

Rosenthal, Y., Lear, C. H., Oppo, D. W., & Linsley, B. K. (2006). Temperature and carbonate ion effects on Mg/Ca and Sr/Ca ratios in benthic foraminifera: Aragonitic species Hoeglundina elegans. *Paleoceanography*, *21*, 1–14. https://doi.org/10.1029/2005PA001158

Skirbekk, K., Hald, M., Marchitto, T. M., Junttila, J., Kristensen, D. K., & Sørensen, S. A. (2016). Benthic foraminiferal growth seasons implied from Mg/Ca-temperature correlations for three Arctic species. *Geochemistry, Geophysics, Geosystems*, *17*, 4684–4704. https://doi.org/10.1002/2016GC006505

Stein, R., Matthiessen, J., Niessen, F., Krylov, A., Nam, S. I., & Bazhenova, E. (2009). Towards a better (litho-) stratigraphy and reconstruction of quaternary paleoenvironment in the Amerasian basin (Arctic Ocean). *Polarforschung*.

Thomsen, V., Schatzlein, D., & Mercuro, D. (2003). Limits of detection in spectroscopy. *Spectroscopy*, *18*(12), 112–114.

Xiao, W., Polyak, L., Wang, R., Löwemark, L., Mei, J., & You, D. (2020). Middle to Late Pleistocene Arctic paleoceanographic changes based on sedimentary records from Mendeleev Ridge and Makarov Basin. *Quaternary Science Reviews*. https://doi.org/10.1016/j.quascirev.2019.106105

Yamada, K., Irizuki, T., Ikehara, K., & Okamura, K. (2014). Calibration of past water temperature in the Sea of Japan based on Mg/Ca of ostracode shells of two shallow marine species in the genus *Cytheropteron*. *Palaeogeography, Palaeoclimatology, Palaeoecology*, *410*, 244–254. https://doi.org/10.1016/j.palaeo.2014.05.042

Yu, J., & Elderfield, H. (2008). Mg/Ca in the benthic foraminifera Cibicidoides wuellerstorfi and Cibicidoides mundulus: Temperature versus carbonate ion saturation. *Earth and Planetary Science Letters*, *276*, 129–139. https://doi.org/10.1016/j.epsl.2008.09.015

Zhang, Z. (2004). *Report of the second Chinese national Arctic expedition (in Chinese)*. Beijing: China Ocean Press.

Zhang, T., Wang, R., Polyak, L., & Xiao, W. (2019). Enhanced deposition of coal fragments at the Chukchi margin, western Arctic Ocean: Implications for deglacial drainage history from the Laurentide Ice Sheet. *Quaternary Science Reviews*, *218*, 281–292.